A Graph-Based Mobility Model for Electric Vehicles in Urban Traffic Networks: Application to the Grenoble Metropolitan Area

Martin Rodriguez-Vega, Carlos Canudas de Wit, Giovanni de Nunzio, Bassel Othman

A Graph-Based Mobility Model for Electric Vehicles in Urban Traffic Networks: Application to the Grenoble Metropolitan Area

Martin Rodriguez-Vega[1], Carlos Canudas-de-Wit[1], Giovanni De Nunzio[2], and Bassel Othman[2]

***Abstract*— This paper introduces a new model depicting electric vehicles (EVs) mobility and the evolution of their State-of-Charge (SoC) in urban traffic networks. The model couples the vehicles' mobility described by a set of dynamic equations over a graph capturing the Origin-Destination motion, with the energy consumption associated with the EVs mobility patterns. Additionally, power inputs from charging stations are included in the model. A model calibration method based on multi-source public data is also provided. Finally, several experiments are conducted through simulation to evaluate the appropriateness of the current charging station infrastructure under an increasing EVs penetration rate in the whole metropolitan area of Grenoble, France.**

I. Introduction

Electric vehicles have become one of the main solutions proposed worldwide in the search for more sustainable and decarbonized transportation. As vehicle electrification is ongoing, several countries have now introduced plans to achieve a carbon-neutral transportation network in the upcoming decades, with EVs replacing conventional vehicles being the main component of this transition. However, the increase in the number of EVs requires a fast adaptation of charging infrastructure, and suitable management of the interaction between the power network [1] and EVs energy demand to avoid overloading the grid nodes during high charging demand periods. Vehicle-to-Grid (V2G) is an existing technology playing a fundamental role to leverage the use of EVs flexibility and promoting the EVs arrival to the markets. Initiatives in that direction have been already taken in cities like Utrecht, which has become a proving ground for the bidirectional-charging techniques that have the rapt interest of automakers, engineers, city managers, and power utilities over the world (see [2]).

To promote the use of V2G technologies, and to better design the charging infrastructure, it is first needed to model the power needs and consumption of EVs in time and space over typical mobility patterns. By doing this, it will be possible to predict the location and time-varying profile of the energy demand and supply sources. Concerning the modeling of SoC and energy expenditure of EVs along their trip, we can find several studies already reported in the literature. [3]–[6] have studied the energy consumption of single vehicles along their trajectories. [7] introduces a microscopic simulator to track the energy consumption of EVs in real-world conditions, taking into account the traffic flow. Macroscopic traffic models that take into account EVs SoC have also been introduced for the case of highways. [8] uses a second-order traffic model to track vehicle speeds and acceleration used to compute the energy consumption. More recently, [9] incorporates a coupled set of PDEs for vehicle density and SoC.

Mobility models describe the movements of individuals in space and time and are important in many disciplines [10]. For instance, [11] used a mobility model to describe the epidemic spread of disease between sectors of an urban area. As the movement and therefore the energy consumption of EVs is obviously linked with the mobility of people, a coupled description of mobility and SoC is needed to provide an accurate view of where EVs energy and power demand are distributed in time and space. However, to the authors' knowledge, there are no works in the literature that model the union between human mobility and EVs SoC. The main contribution of this paper is the introduction of a graph-based electromobility model including the SoC of the EVs. The model starts with the urban human mobility model developed previously [11] in the context of the ERC project Scale-FreeBack [12]. Our contribution here is first to split the people flows into several transportation modes including EVs. Secondly, we have added an energy model, that tracks the energy lost by the EVs during the trip. For that, we have introduced the concept of power flow instead of vehicle flow typically used in people's mobility alone. The model has been completed with the consideration of energy provided by public and private charging stations.

This model is used to track the SoC and energy EVs at different locations of an urban area, as well as the possible flexibility that can be used in V2G scenarios. In this paper, we use to model to determine the effect of several EVs penetration rates and charging configurations on the SoC of vehicles, to determine the maximum possible number of EVs that can be maintained in a metropolitan area.

The paper is organized as follows: Section II presents the electromobility model and describes its main components. Section III presents the study case of the Grenoble metropolitan area, and the data sources used to calibrate and run the model. Two experiment scenarios and their results are presented in Sections IV and V, using the model to predict the maximum EVs penetration rate that can be supported in the area using different charging infrastructures. Finally, Section VI concludes the paper.

[1] Univ. Grenoble Alpes, CNRS, INRIA, Grenoble INP, GIPSA-Lab, 38000 Grenoble, France {martin.rodriguez-vega1@gipsa-lab.fr, carlos.canudas-de-wit}@cnrs.fr

[2] IFP Energies nouvelles, Rond-point de l'échangeur de Solaize, BP 3, 69360 Solaize, France. {giovanni.de-nunzio, bassel.othman}@ifpen.fr

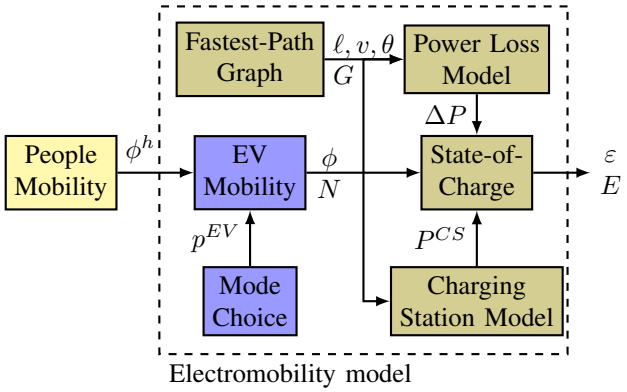

Fig. 1: Overview of the Electromobility Model.

II. Electromobility model

The Electromobility model is seeking to capture the dynamic motion of the EVs distribution and their state of charge within a given area by using a dynamic graph formulation. The mobility part of the model is described by a bipartite graph (only round trips are considered here) structure which provides information on how and when the people move during a journey from a set of origin nodes to a set of destination nodes and back again. The origins correspond to the aggregated residential areas in a municipality, whereas the destination nodes include five classes of destinations: schools, workplaces, hospitals, shopping areas, and leisure. The model states are: the number of EVs in each node $N_i(t)$, the EVs flow between nodes i and j, $\phi_{i,j}(t)$ [veh/h], the normalized average State-of-Charge of the EVs at each node $\varepsilon_i(t) \in [0, 1]$, and the total energy contained by all the EVs in a node $E_i(t)$.

The model consists of seven modules as shown in Fig. 1. The fastest-path graph module computes the paths used by EVs to move between nodes and their parameters such as length and average speed. The people mobility module computes the number of people at each node and provides the flow ϕ^h between nodes. The mode choice module computes the proportion of people using EVs and feeds this information to the EVs mobility module which transforms people's mobility into EVs mobility. This module's output (EVs number N and flow ϕ) are inputs for the other modules. The power losses module computes the aggregated losses, ΔP, on a trip from one node to another. The charging station model module computes the aggregated power injected at each station. Finally, the State-of-Charge module computes the aggregated SoC and energy of the EVs in each node.

A detailed description of each module is presented in the next subsections.

A. People mobility module

To model the people's mobility we use the model introduced in [11], which is based on a set of coupled conservation Ordinary Differential Equations (ODEs) of the form

$$\dot{N}_i^h(t) = \sum_j (\phi_{j,i}^h(t) - \phi_{i,j}^h(t)) \tag{1}$$

where N_i^h corresponds to the number of people in node i, and $\phi_{i,j}^h$ is the flow of people from node i to node j. For details on the flow functions, input data, and implementation, interested readers can find more details in [11], [13], where the model was extended and applied to the Grenoble urban metropolitan area.

B. Fastest-path graph module

This module produces a graph G, that for each combination of origin node i and destination node j, defines the topology of the path (x, y coordinates) that minimizes the free-flow traveling time of vehicles moving between i and j. The path topology is used in the charging station module to determine which public chargers are used by EVs in the path.

Furthermore, for each path we compute the length $\ell_{i,j}$, the average vehicle speed $v_{i,j}$, and the average road inclination $\theta_{i,j}$. The latter is computed as

$$\theta_{i,j} = \arctan((h_j - h_i)/\ell_{i,j}) \tag{2}$$

where h_i is the elevation of node i. These physical parameters are used in the power loss module.

C. Mode choice module

To transform people's mobility into EVs mobility, we need to compute first the proportion of people using a private car. This problem is known as the modal choice analysis and has been extensively studied in the literature, see [14], [15]. Here we adopt the well-known logit model which computes the probability that a person uses their private vehicle (rather than public transport) as

$$p^{car}(\Delta t) = \frac{1}{1 + \exp(\beta_0 + \beta_1 \Delta t)} \tag{3}$$

where $\Delta t \in \mathbb{R}$ is the traveling time difference between public transport and private cars. In this study we use only this descriptor variable because it has been demonstrated to be the most representative and relatively easy to compute [16], [17], but more general forms can be adopted as well, considering multiple descriptor variables and modes of transport, see [14]. The constants parameters $\beta_0, \beta_1 \in \mathbb{R}$ are adjusted using public mobility data as it will be explained in Section III.

D. EVs mobility module

Once the number of cars performing each trip is known, the corresponding number of EVs, N_i, can be computed using the penetration rate η. From the mass conservation property, we have:

$$\dot{N}_i(t) = \sum_j (\phi_{j,i}(t) - \phi_{i,j}(t)) \tag{4}$$

where

$$\phi_{i,j}(t) = \eta p^{car}(\Delta t_{i,j}) \phi_{i,j}^h(t). \tag{5}$$

E. Power loss module

The total power lost during the EVs displacement from node i to j is described by:

$$\Delta P_{i,j} = \phi_{i,j} E_{i,j}^l \tag{6}$$

where $E_{i,j}^l$ is the average energy lost per vehicle [3],

$$E_{i,j}^l = E^F(\ell_{i,j}, v_{i,j}, \theta_{i,j}) + E^v(v_{i,j}) + E^{aux}(\ell_{i,j}, v_{i,j}) \tag{7}$$

TABLE I: Parameters and notation for power loss model.

Symbol	Description	Units	Value
m	Vehicle mass	kg	1700
A	Vehicle frontal area	m^2	2.33
g	Gravity acceleration	m/s^2	9.81
c_r	Roll friction coeff.	-	0.01
c_d	Air drag friction coeff.	-	0.3
ρ_{air}	Air density	kg/m^3	1.2
μ_{mot}	Battery-to-wheels efficiency	-	0.65
μ_{reg}	Regenerative braking efficiency	-	0.55
P^{aux}	Power used by auxiliary systems	kW	0.7
C	Average EVs battery capacity	kWh	40

where the first term, E^F, represents the losses due to external forces from $i \mapsto j$, and has the following general form:

$$E^F(\ell, v, \theta) = \begin{cases} \frac{1}{\mu_{mot}} \ell F(v,\theta) & \text{if} \quad F(v,\theta) \geq 0 \\ \mu_{reg} \ell F(v,\theta) & \text{if} \quad F(v,\theta) < 0 \end{cases} \tag{8}$$

where ℓ, v, θ are the trip's length, average vehicle speed, and road inclination, respectively. $F(v,\theta)$ is the force required at the wheels to keep a constant speed v against gravity and drag forces,

$$F(v,\theta) = (\sin\theta + c_r \cos\theta) mg + \frac{1}{2} \rho_{air} A c_d v^2 \tag{9}$$

where the parameters are given in Table I. When $F(v)$ is positive (energy is lost), the power supplied by the battery is higher than the power used at the wheels. When $F(v)$ is negative (energy is recovered), the battery converts a part of the braking power to charge itself.

The second term in (7), E^v, is the kinetic energy needed to reach a speed v without consideration of energy losses,

$$E^v(v) = \frac{1}{2} \left(\frac{1}{\mu_{mot}} - \mu_{reg} \right) m v^2. \tag{10}$$

Finally, the last term in (7), E^{aux}, is the energy used by auxiliary vehicle systems (e.g. air conditioning) given by

$$E^{aux}(\ell, v) = \frac{\ell}{v} P^{aux} \tag{11}$$

where P^{aux} is the constant power used by the auxiliary systems.

F. Charging station module

To model the power injected by charging stations, we consider three types of chargers: *a)* Home Chargers (HC), *b)* Office Chargers (OC), and *c)* Public Chargers (PC).

1) Home chargers: These chargers are only present at origin nodes (residential) and their injected power is modeled as,

$$P_i^{HC} = \begin{cases} P_{HC}^{avg} \min(N_i, N_i^{HC}) \psi_i & \text{if} \quad \varepsilon_i < \varepsilon^{max} \\ 0 & \text{else} \end{cases} \tag{12}$$

where P_{HC}^{avg} is the average power per charger, and N_i^{HC} is the number of HC in node i. We assume that vehicles do not charge above $\varepsilon^{max} \leq 1$ to protect the battery, and $\psi_i(t)$ specifies the time window when vehicles can charge at home during the night, i.e.

$$\psi_i(t) = \begin{cases} 1 & \text{if} \quad t \in [20{:}00, 6{:}00] \\ 0 & \text{else} \end{cases}.$$

2) Office chargers: These chargers are available at destination nodes at workplaces and shopping areas. The supply power from OC follows the same model as HC, namely

$$P_j^{OC} = \begin{cases} P_{OC}^{avg} \min(N_j, N_j^{OC}) \psi_j & \text{if} \quad \varepsilon_j < \varepsilon^{max} \\ 0 & \text{else} \end{cases} \tag{13}$$

where P_{OC}^{avg} is the average charger power, and N_j^{OC} is the number or chargers at location j. The time window $\psi_j(t)$ for destination nodes is

$$\psi_j(t) = \begin{cases} 1 & \text{if} \quad t \in [9{:}00, 18{:}00] \\ 0 & \text{else} \end{cases}.$$

3) Public access chargers: These chargers are used by vehicles during their transit between nodes. We assume that the location and average power per station of the PC in the area are given.

As the PC are not necessarily located over a specific Origin-Destination (OD) link but rather in their neighborhood, we need to define how those charges will contribute to supplying power to each of the links in the graph. For that, we first specify which PC will provide power to each graph's link. For that, we use a gravity attraction law (see [10]) depending on one hand on the shortest distance between the PC geographic location of the link's graph, and on the other, on the average power supply capacity of each station. The rationality behind this model is that drivers will be more "attracted" to close PC locations with enough power availability.

We denote by $d_{i,j}^k$ as the shortest distance between PC k and the path between nodes i and j, see Fig. 2. Also, denote by $\ell_{i,j}^k$ as the distance between node i and the closest point to PC k along the path (i,j).

We define the attraction between the link and the PC as

$$A_{i,j}^k = P_k^{avg} \exp\left(-\left(\frac{d_{i,j}^k}{\sigma} \right)^2 \right) \tag{14}$$

where P_k^{avg} is the average power charging station capacity, and σ is the distance that people are willing to deviate from their original destination path to go for a charge. Now,

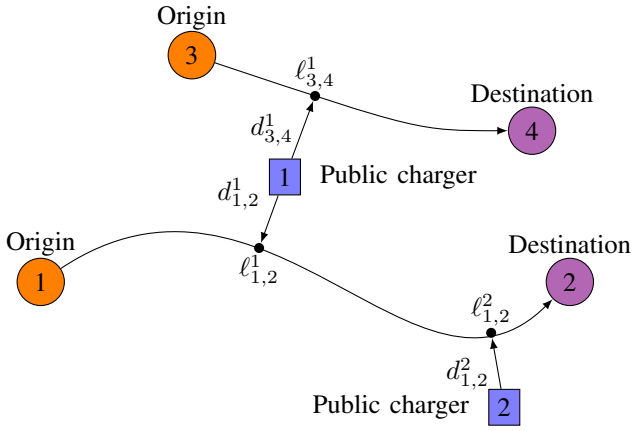

Fig. 2: Example with 2 OD paths and 2 PC. The arrows from the PC to the path indicate if the PC supplies power to EVs making this trip according to the "attraction" between the PC and the path. $\delta_{i,j}^k$ is the distance between PC k and the path (i,j), and $\ell_{i,j}^k$ is the distance from i to k along the path towards j.

introducing the normalized attraction law,

$$\bar{A}^k_{i,j} = \frac{A^k_{i,j}}{\max_n(A^n_{i,j})}. \tag{15}$$

and the design threshold parameter τ, we say PC k is connected to (i,j) if $\bar{A}^k_{i,j} \geq \tau$. For example, Fig. 2 shows that PC 1 is connected to links $(1,2)$ and $(3,4)$. Conversely, PC 2 is only connected to link $(1,2)$, as link $(3,4)$ is too far away.

This process is repeated for all links and PC. This provides the set $\Omega_{(i,j)}$ of all charging stations connected to link (i,j), and set Γ_k of all paths connected to charging station k.

The power provided by each station to each connected link is computed as

$$P^k_{i,j} = \min(D^k_{i,j}, S^k_{i,j}) \tag{16}$$

where the demand D specifies the maximum power that the flow of vehicles in the route can receive and is computed by

$$D^k_{i,j} = C\phi_{i,j}(\varepsilon^{max} - \varepsilon_i) + \frac{\ell^k_{i,j}}{\ell_{i,j}}\Delta P_{i,j} - \sum_{\substack{p\in\Omega_{(i,j)} \\ \ell^p_{i,j}<\ell^k_{i,j}}} P^p_{i,j} \tag{17}$$

where C is the average EVs battery capacity. The first term is the power needed to raise the SoC of the flow to ε^{max}, the second term is the power loss due to the EVs movement, and the last term is the power already provided by connected PC upstream.

The supply S specifies how much power can be provided by the PC. If it is connected to multiple routes, the maximum power is divided proportionally according to the energy needs of each route,

$$S^k_{i,j} = \alpha^k_{i,j} P^{tot}_k \tag{18}$$

where

$$\alpha^k_{i,j} = \frac{\phi_{i,j}(\varepsilon^{max} - (\varepsilon_i - \varepsilon^k_{i,j}))}{\sum_{(n,m)\in\Gamma_k} \phi_{n,m}(\varepsilon^{max} - (\varepsilon_n - \varepsilon^k_{n,m}))} \tag{19}$$

such that $\sum_{(i,j)\in\Gamma_k} \alpha^k_{i,j} = 1$, P^{tot}_k is the total power from points in the station, and $\varepsilon^k_{i,j} = (E^l_{i,j}\ell^k_{i,j})/(C\ell_{i,j})$.

4) Power in each node from all chargers contributions: For each origin node i, the total received power from charging is the sum of the contributions from home chargers and public chargers located in the D/O paths,

$$P^{CS}_i(t) = P^{HC}_i(t) + \sum_j \sum_{k\in\Omega_{(j,i)}} P^k_{j,i}(t) \tag{20}$$

and for each destination node j the total received power from charging is the sum of the contributions from office chargers and public chargers located in the O/D paths,

$$P^{CS}_j(t) = P^{OC}_j(t) + \sum_i \sum_{k\in\Omega_{(i,j)}} P^k_{i,j}(t). \tag{21}$$

G. State-of-Charge module

The dynamics of the energy stored by EVs in node i is given by a conservation law

$$\dot{E}_i(t) = P^{CS}_i(t) + \sum_j (P^{in}_{j,i}(t) - P^{out}_{i,j}(t)) \tag{22}$$

where $P^{in}_{j,i}$ is the power flow entering node i from j, $P^{out}_{i,j}$ is the power flow exiting node i towards j. The energy in each node is given in terms of the SoC,

$$E_i(t) = CN_i(t)\varepsilon_i(t) \tag{23}$$

and the power transported out by EVs is

$$P^{out}_{i,j}(t) = C\phi_{i,j}(t)\varepsilon_i(t). \tag{24}$$

The power entering each node takes into account the link losses

$$P^{in}_{i,j} = P^{out}_{i,j} - \Delta P_{i,j}. \tag{25}$$

Note that from (23),

$$\dot{E}_i = C(\dot{N}_i\varepsilon_i + N_i\dot{\varepsilon}_i). \tag{26}$$

Substitution of (4), (6), (24), (25), and (26) into (22) and rearranging terms gives

$$\dot{\varepsilon}_i = \frac{1}{N_i}\left(\frac{P^{CS}_i}{C} + \sum_j \left(\phi_{j,i}(\varepsilon_j - \varepsilon_i) - \frac{\Delta P_{j,i}}{C}\right)\right). \tag{27}$$

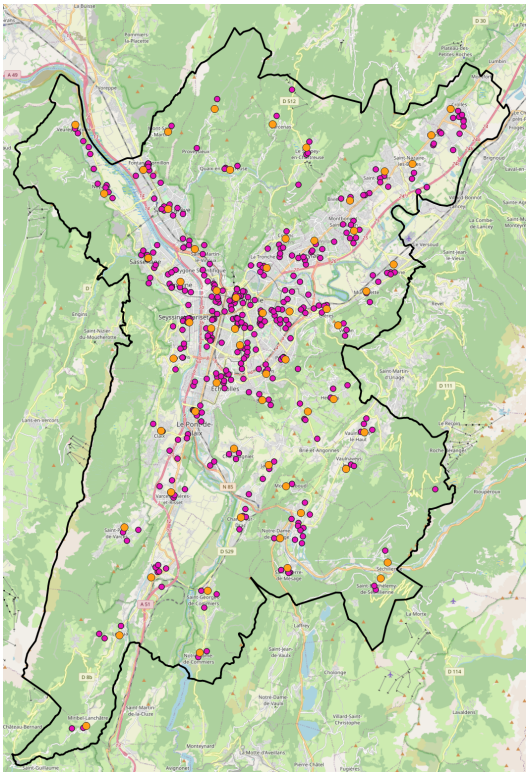

Fig. 3: Layout of the Grenoble metropolitan area. Large orange circles represent Origin nodes; small purple circles are Destination nodes.

III. Model Parameter Calibration

The model is calibrated for the Grenoble metropolitan area in the French Alps, whose boundaries are shown in Fig. 3. Highlighted in orange are the 60 origin nodes representing the municipalities. Highlighted in purple are the 374 destination nodes. The population in the area is approximately 470.000 people.

Calibration is performed using data sources and algorithms exclusively from public government agencies and open source repositories, see Table II.

TABLE II: Data sources description for parameter calibration.

Source name	Source type	Function	Data	Ref.
INSEE	National institute of statistics	Calibration of people mobility	Node population and capacity	[18]
CEREMA, SMMAG	Mobility and Urbanism agencies of Grenoble-Alpes region	Calibration of mode choice model, and number of HC per node.	Household mobility survey EMD2010: inter municipality trips, and type of parking used.	[19]
OpenStreetMaps, OSMnx	Open source data and algorithms	Computation of car trajectories and traveling time.	Car road graphs and fastest-path calculation algorithms.	[20]
SMMAG	Mobility agency of Grenoble-Alpes region	Computation of public transport traveling times.	Public transport map and itineraries.	[21]
OpenTripPlanner	Open source algorithms	Computation of public transport traveling times	Fastest path algorithm.	[22]
MERIT-DEM	Open source data	Road inclination computation for energy loss.	Digital Elevation Map	[23]
ENEDIS	French energy distribution system operator.	Calibrate the number and power of chargers.	Number of chargers of each type at the national level and total power.	[24]
OpenChargeMap	Open source data	Input data for PC.	PC location and nominal power.	[25]
Ministry of Ecological Transition	Public organism	Initial condition for EVs distribution	Number of vehicles, EVs and penetration rate per municipality.	[26]

A. Fastest-path calculation

To compute the paths between origin and destination nodes, we compute the road network graph using the fastest-path algorithm OSMnx [20] with input data from OpenStreetMaps. The paths are given as a set of point coordinates, and the lengths and traveling times between consecutive points are also provided by the algorithm. Node elevations were obtained from [23]. We used the road network graph and the fastest-path algorithm implemented in OSMnx [20] using the free-flow traveling time.

B. Mode choice

The parameters β_0 and β_1 depend on the destination class. For calibration, the household survey EMD2010 [19] data is used. This dataset divides the metropolitan area into sectors and provides the number of people using car or public transport according to: the origin and destination sectors, and destination class. Although the sectors defined in the EMD2010 do not match exactly with the nodes used in the electromobility model, the parameters calibrated with the EMD2010 data will be used in the electromobility model as they consider the same population. A sample n of the EMD2010 is comprised of the proportion of surveyed people using car p_n^{car} for an OD pair and destination class, and the average travel time difference Δt_n is computed using OSMnx [20] for cars, and OpenTripPlanner [22] for public transport.

The parameters β_0, β_1 were calibrated using a least-squares approach [27]. For this, we transform (3) into

$$\log\left((1-p^{car})/p^{car}\right) = \beta_0 + \beta_1 \Delta t. \tag{28}$$

Define $y_n = \log((1-p_n^{car})/p_n^{car})$, which can be computed from data. As both variables y_n and Δt_n are noisy, we use a error-in-the-variables linear regression method known as Deming regression [28],

$$\min_{\beta_1,\beta_0,x_n} \quad \sum_n ((y_n - \beta_0 - \beta_1 x_n)^2 + \delta(\Delta t_n - x_n)^2) \tag{29}$$

where x_n are dummy variables and δ is the ratio between sample variances of y_n and Δt_n. The resulting values are shown in Table III.

TABLE III: Parameters for the mode choice model.

Destination class	β_0	β_1 [1/min]
Workplaces	2.35	-0.11
Schools	5.17	-0.11
Leisure, Shopping	2.82	-0.11
Hospitals	3.43	-0.13

C. Number of EVs by municipality

The current distribution of EVs number and penetration rate by municipality can be seen in Fig. 4, obtained from the Ministry of Ecological Transition [26]. Note from the right figure that most of the EVs are concentrated in the center of the area (corresponding to the capital city of Grenoble), and an axis towards the northeast of Grenoble. The city of Grenoble, however, has a lower penetration rate, as it contains a larger vehicle population. The northeast axis, although having fewer total vehicles, have a similar number of EVs, as evidenced by a higher penetration rate.

It can be seen that some areas in the north have very high penetration rates compared to the rest of the map. However, these areas have very few vehicles in total, so the high penetration values might be artificially high.

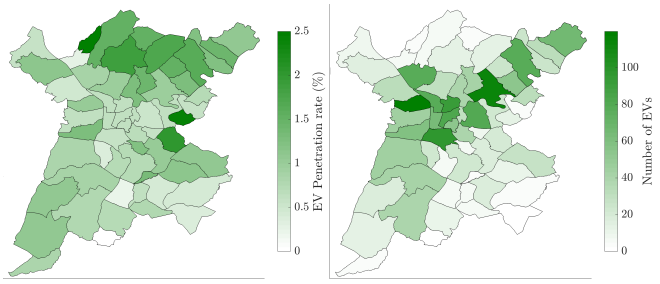

Fig. 4: Current spatial distribution of the number of EVs and penetration rate by municipality.

D. Charging stations

1) Public chargers: the locations of the PC are shown in Fig. 5 as obtained from OpenChargeMap [25]. The total number of PC and the average power per point are shown in Table IV. To determine which PC contributes to each link, we use the process described in Section II-F with the paths

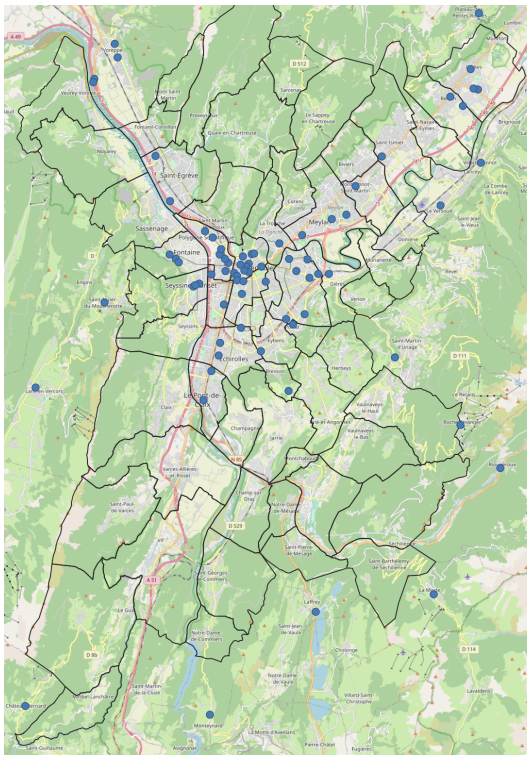

Fig. 5: Location of PC, and municipality outlines.

computed using OSMnx [20] and the heuristic parameters $\sigma = 0.3$km, $\tau = 0.8$.

2) Home chargers: To estimate the number of HC in each municipality, N_i^{HC}, we use parking data from EMD2010 [19], which indicates the proportion of vehicles that park during the night in private garages, shared parking, or at the roadside. We assume that EVs with access to a private garage have access to an HC. Thus, we estimate N_i^{HC} by multiplying the proportion of vehicles that park in garages by the total number of EVs registered in municipality i. The average power per HC as obtained from ENEDIS [24] is 2 kW, as seen in Table IV.

3) Office chargers: To estimate the number of OC, N_i^{OC}, we use the data provided by ENEDIS [24], which specifies the ratio between the number of PC and the number OC at a national level. As the number of PC in the area is known, the total number of OC is calculated proportionally. For each destination node, the number of OC is distributed in proportion to the node capacity. The average power per OC as obtained from ENEDIS [24] is 7 kW, as seen in Table IV.

Table IV shows the total number of charging points, the total available power, and the average power per point for the three categories.

Figure 6 shows snapshots of the spatial-temporal time evolution of the model in a working journey. Note how the

TABLE IV: Number and power characteristics of charging stations.

Type	Points	Total Power	Avg power/point
Home	1306	2612 kW	2 kW
Office	1220	8540 kW	7 kW
Public	236	4720 kW	20 kW

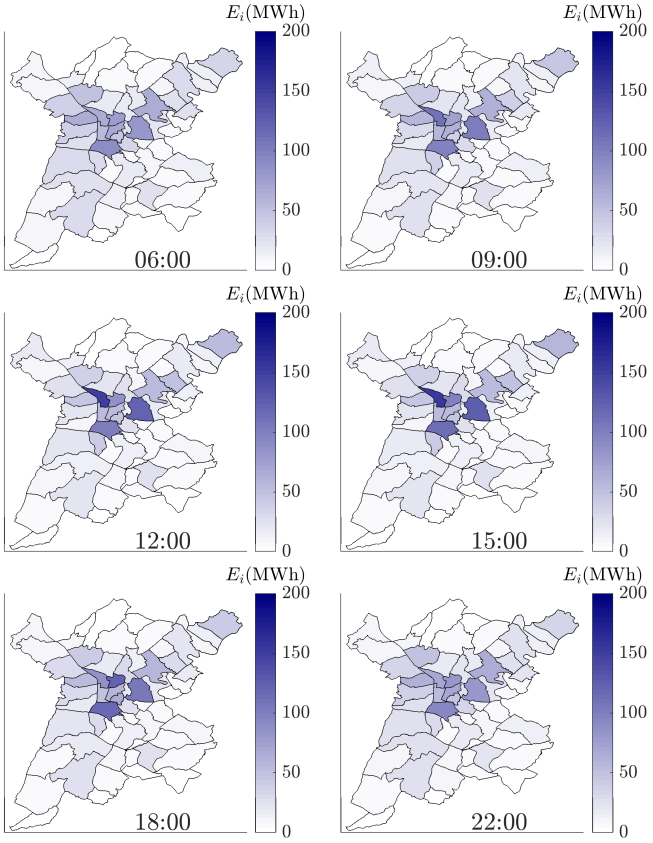

Fig. 6: Spatial distribution of Energy (MWh) in each municipality at different times of the day, for a penetration rate of 22%.

energy concentrates at the center of the area during working hours, due to the mobility of people, and then disseminates back to the residential areas during the night.

IV. Study Case 1: Phase-Transition EVs Penetration Rate for Sustainable Charging

In this first study case, we consider the current Grenoble charging station network, as described in Section III-D. The objective is to determine the EVs penetration rate η^* at which the charging station network can no longer meet the energy demand of EVs (phase transition value). Several simulations with an increasing penetration rate of EVs are carried out.

We consider the overall average SoC of all EVs in the network as

$$\bar{\varepsilon}(t) = \frac{\sum_i N_i(t)\varepsilon_i(t)}{\sum_i N_i(t)}. \tag{30}$$

Simulations are performed using several initial conditions and penetration rates. Fig. 7 shows the trajectories of $\bar{\varepsilon}(t)$ from an initial condition $\bar{\varepsilon}(0) = 0.4$, where each color corresponds to a different η. We note three cases: *a)* for $\eta < 0.22$, $\bar{\varepsilon}$ increases and then remains around a value close to 1; *b)* for $\eta > 0.22$, $\bar{\varepsilon}(t)$ decreases until vehicles are discharged; and *c)* for $\eta = 0.22$, $\bar{\varepsilon}(t)$ oscillates around the initial value. Thus, there exists a phase-transition value $\eta^* = 0.22$ that differentiates between sustainable charging and discharging of vehicles.

Figure 8 shows the phase portrait of $\bar{\varepsilon}(t)$ vs η. The plot is divided into several regions according to the behavior

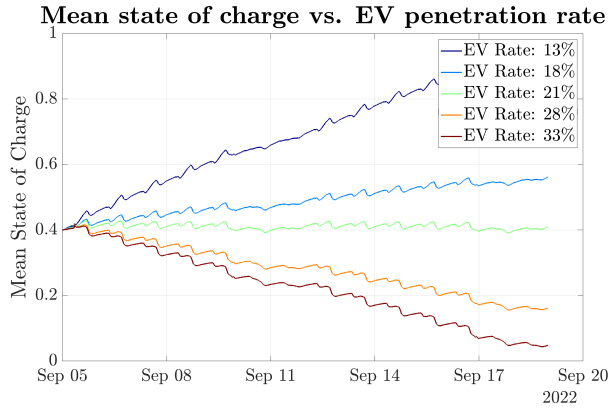

Fig. 7: Evolution of the mean state of charge with varying EV changing penetration rates.

of the trajectory. The black band is an attractive invariant set, i.e., initial conditions (ICs) taken outside of the band will converge towards the band and will remain there (with eventually small oscillations). The arrows in the figure shows the direction of trajectories starting above or below the invariant set. Thus, three main sub-regions are identified: ICs starting in the green sub-region will increase $\bar{\varepsilon}(t)$ until reaching the band; ICs starting in the blue region decrease $\bar{\varepsilon}(t)$ until reaching the band; and ICs starting in the red region will decrease $\bar{\varepsilon}(t)$ until vehicles are discharged.

V. Study Case 2: Dependency of the Phase-Transition Penetration Rate on the Home and Office Chargers Number

As more people adopt EVs, even past the current phase-transition penetration rate, the supply of the charging network needs to be augmented to sustain the rising energy needs. In this study case, we analyze the number of chargers at homes, N^{HC}, and at offices, N^{OC}, that would be required to meet the energy demands of EVs for a given penetration rate. To do this, we simulate different configurations of charging networks by independently varying N^{HC} and N^{OC}, without changing the average power per charger shown in Table IV. For each new configuration, we determine the new value η^*.

Fig. 9 shows the values of η^* for charging configuration.

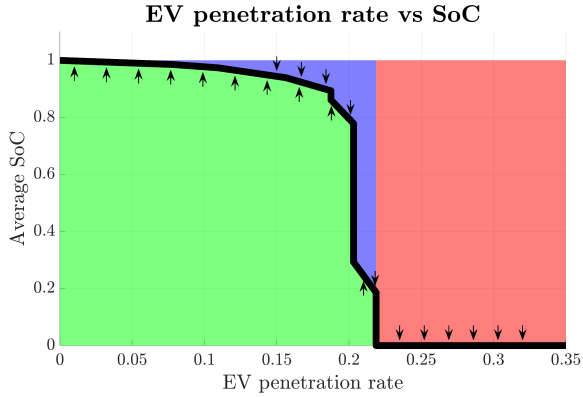

Fig. 8: Behavior of the average SoC trajectories according to the penetration rate and initial conditions. The black line is an attractive invariant set, as all points move vertically toward the line. Points in the red region will move towards 0.

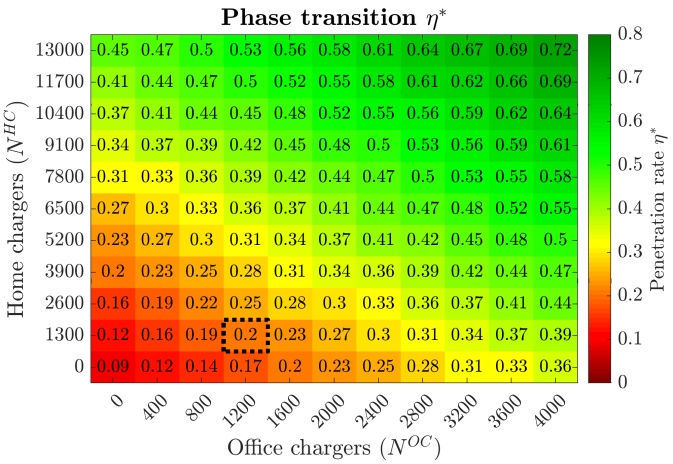

Fig. 9: Phase-transition penetration rate for varying numbers of home and office chargers.

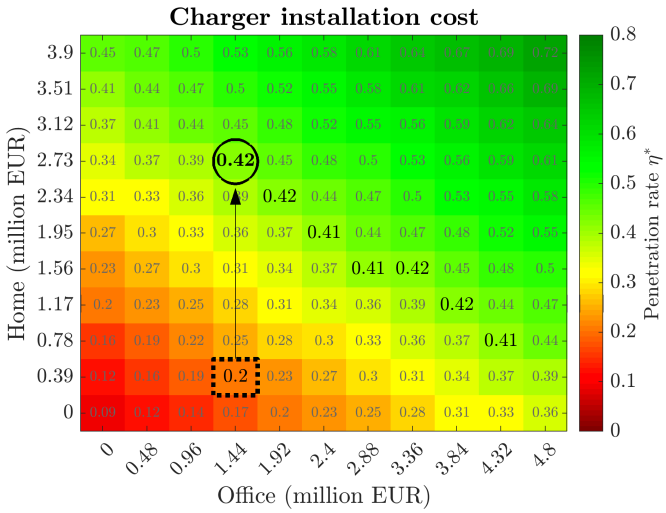

Fig. 10: η^* according to HC and OC installation costs. The circle corresponds to the configuration with the lowest cost increment to achieve $\eta^* = 0.42$

The square highlighted with the dotted black line corresponds to the current charging network (the same as in study case 1). Consider for instance the case when we would like to augment the penetration rate to 42%. In the figure, this value corresponds to the situation $N^{HC} = 2612$ and $N^{OC} = 1830$. However, note that this configuration is not unique, and in fact, as isolines of constant η^* can be evidenced.

An interesting problem is to determine the optimal configuration for a given η^*, such that the installation cost (for instance) is minimized. The figure shows that adding a certain N^{OC} yields a better increase in η^* than the same N^{HC}. However, HC are usually cheaper, with an installation cost of approx. 300 EUR, vs an installation cost of 1200 EUR for OC. Fig. 10 shows the resulting η^* that corresponds to the installation cost for each configuration. Note that for obtaining the same η^*, augmenting N^{HC} rather than N^{OC} results in lesser costs. For this scenario, the circle corresponds to the configuration that minimizes the installation for $\eta^* = 42\%$, with an extra cost of 2.34M€.

VI. Conclusions

In this paper, we have introduced the Electromobility model, which describes the SoC dynamics of EVs in an urban area taking into account the mobility of the EV population, their energy consumption, and the power inputs from charging stations. This model consists of a set of coupled ODE based on flow and energy conservation law on the nodes of an origin-destination graph. We have also presented a method to calibrate the model parameters using publicly available data sources and showcased this for the specific case of the Grenoble metropolitan area. The model was used to compute the phase-transition penetration rate of EVs such that different charging infrastructures could satisfy the energy demand of vehicles. For future work, this model can be used as an input to determine the optimal location of public chargers, and control schemes to reduce the power peaks on charging stations under power grid constraints.

Acknowledgements

This project has received funding from the European Research Council (ERC) under the European Union's Horizon 2020 research and innovation programme (grant agreement 694209), see [12].

References

[1] A. Klettke and A. Mose, "Effect of electromobility on the power system and the integration of RES," European Commission, Directorate-General for Energy, Tech. Rep., 2019. [Online]. Available: https://data.europa.eu/doi/10.2833/12919

[2] M. Dumiak, "This dutch city is road-testing vehicle-to-grid tech," 2022. [Online]. Available: https://spectrum.ieee.org/vehicle-to-grid

[3] C. Fiori, K. Ahn, and H. A. Rakha, "Power-based electric vehicle energy consumption model: Model development and validation," *Applied Energy*, vol. 168, pp. 257–268, 2016.

[4] Y. Al-Wreikat, C. Serrano, and J. R. Sodré, "Driving behaviour and trip condition effects on the energy consumption of an electric vehicle under real-world driving," *Applied Energy*, vol. 297, no. May, 2021.

[5] B. Luin, S. Petelin, and F. Al-Mansour, "Microsimulation of electric vehicle energy consumption," *Energy*, vol. 174, pp. 24–32, 2019.

[6] A. Pirayre, P. Michel, S. S. Rodriguez, and A. Chasse, "Driving Behavior Identification and Real-World Fuel Consumption Estimation With Crowdsensing Data," *IEEE Transactions on Intelligent Transportation Systems*, vol. 23, no. 10, pp. 18 378–18 391, 2022.

[7] P. Raimondo, A. F. Santamaria, F. D. Rango, and A. Bosco, "A vehicular traffic simulator model for evaluating electrical vehicles (evs) performances in a configurable mobility scenario," *SIMULTECH 2018 - Proceedings of 8th International Conference on Simulation and Modeling Methodologies, Technologies and Applications*, no. Simultech, pp. 198–205, 2018.

[8] M. Ross, L. Du, and B. Seibold, "Spatial-temporal EV charging demand model considering generic second-order traffic flows," *2021 IEEE Transportation Electrification Conference and Expo, ITEC 2021*, pp. 789–794, 2021.

[9] M. Čičić and C. Canudas-de-Wit, "Coupled Macroscopic Modelling of Electric Vehicle Traffic and Energy Flows for Electromobility Control To cite this version : HAL Id : hal-03760831 Coupled Macroscopic Modelling of Electric Vehicle Traffic and Energy Flows for Electromobility Control," in *CDC 2022 - 61st IEEE Conference on Decision and Control*, Cancun, Mexico, 2022.

[10] H. Barbosa, M. Barthelemy, G. Ghoshal, C. R. James, M. Lenormand, T. Louail, R. Menezes, J. J. Ramasco, F. Simini, and M. Tomasini, "Human mobility: Models and applications," *Physics Reports*, vol. 734, pp. 1–74, 2018.

[11] M. U. B. Niazi, C. Canudas-de-Wit, A. Kibangou, and P.-A. Bliman, "Optimal Control of Urban Human Mobility for Epidemic Mitigation," in *2021 60th IEEE Conference on Decision and Control (CDC)*. IEEE, dec 2021, pp. 6958–6963.

[12] "Scale-Free Control for Complex Physical Network systems. Scale-FreeBack." [Online]. Available: http://scale-freeback.eu/

[13] U. Pratap, C. Canudas-de-Wit, and F. Garin, "Where , when and how people move in large-scale urban networks : the Grenoble saga," Tech. Rep., 2022. [Online]. Available: https://hal.archives-ouvertes.fr/hal-03554612

[14] H. Bouscasse, I. Joly, and J. Peyhardi, "A new family of qualitative choice models: An application of reference models to travel mode choice," *Transportation Research Part B: Methodological*, vol. 121, pp. 74–91, 2019.

[15] A. Mondal and C. R. Bhat, "A spatial rank-ordered probit model with an application to travel mode choice," *Transportation Research Part B: Methodological*, vol. 155, no. August 2021, pp. 374–393, 2022.

[16] K. Train, "A validation test of a disaggregate mode choice model," *Transportation Research*, vol. 12, no. 3, pp. 167–174, 1978.

[17] F. Southworth, "Calibration of multinomial logit models of mode and destination choice," *Transportation Research Part A: General*, vol. 15, no. 4, pp. 315–325, 1981.

[18] Institut national de la statisque et des études économiques (INSEE), "Local statistics," 2022. [Online]. Available: https://statistiques-locales.insee.fr/

[19] CEREMA and S. mixte des transports en commun de l'agglomération grenobloise, "Enquête Ménages Déplacements, Grenoble / Grande région grenobloise - 2010," 2010. [Online]. Available: https://www.data.gouv.fr/fr/datasets/enquetes-menages-deplacements-emd/

[20] G. Boeing, "OSMnx: New methods for acquiring, constructing, analyzing, and visualizing complex street networks," *Computers, Environment and Urban Systems*, vol. 65, pp. 126–139, 2017.

[21] Syndicat Mixte des Mobilités de l'Aire Grenobloise, "Horaires théoriques du réseau TAG," 2022. [Online]. Available: https://www.data.gouv.fr/fr/datasets/horaires-theoriques-du-reseau-tag/

[22] M. Morgan, M. Young, R. Lovelace, and L. Hama, "OpenTripPlanner for R," *Journal of Open Source Software*, vol. 4, no. 44, p. 1926, 2019.

[23] D. Yamazaki, D. Ikeshima, R. Tawatari, T. Yamaguchi, F. O'Loughlin, J. C. Neal, C. C. Sampson, S. Kanae, and P. D. Bates, "A high-accuracy map of global terrain elevations," *Geophysical Research Letters*, vol. 44, no. 11, pp. 5844–5853, 2017.

[24] ENEDIS, "Nombre total de points de charge," 2022. [Online]. Available: https://data.enedis.fr/

[25] OpenChargeMap, "Open Charge Map." [Online]. Available: https://openchargemap.org

[26] Ministère de la transition écologique et de la cohésion des territoires, "Données sur le parc automobile français au 1er janvier 2021," 2021. [Online]. Available: https://www.statistiques.developpement-durable.gouv.fr/donnees-sur-le-parc-automobile-francais-au-1er-janvier-2021

[27] D. McFadden, "Conditional logit analysis of qualitative choice behavior," in *Frontiers in Econometrics*, P. Zarembka, Ed. Academic Press, 1973, ch. Chapter Fo, pp. 105–142.

[28] C. H. Kummel, "Reduction of Observation Equations Which Contain More Than One Observed Quantity," *The Analyst*, vol. 6, no. 4, pp. 97–105, 1879.